Title

Multipotent bone marrow cell-seeded polymeric composites drive long-term, definitive urinary bladder tissue regeneration.

Journal

PNAS Nexus, 3(2)

Authors

Bury, Matthew
Fuller, Natalie
Wang, Xinlong
et al.

Publication Date

2024-02-01

DOI

10.1093/pnasnexus/pgae038

Peer reviewed

PNAS Nexus, 2024, 3, 1–14
https://doi.org/10.1093/pnasnexus/pgae038
Advance access publication 30 January 2024
Biological, Health, and Medical Sciences

Multipotent bone marrow cell–seeded polymeric composites drive long-term, definitive urinary bladder tissue regeneration

Matthew I. Bury[a,1], Natalie J. Fuller[a,1], Xinlong Wang[b,1], Yvonne Y. Chan[c,1], Renea M. Sturm[d,1], Sang Su Oh[e], Laurel A. Sofer[f], Hans C. Arora[a], Tiffany T. Sharma[a], Bonnie G. Nolan[a], Wei Feng[g], Rebecca R. Rabizadeh[a], Milica Barac[a], Sonia S. Edassery[a], Madeleine M. Goedegebuure[b], Larry W. Wang[h], Balaji Ganesh[g], Lisa C. Halliday[e], Mark E. Seniw[i], Seby L. Edassery[j], Nadim B. Mahmud[k], Matthias D. Hofer[l], Kevin E. McKenna[h,m], Earl Y. Cheng[a,h,i,n,o], Guillermo A. Ameer[b,i,o,p] and Arun K. Sharma[a,b,h,i,n,o,*]

[a]Division of Pediatric Urology, Department of Surgery, Ann & Robert H. Lurie Children's Hospital of Chicago, Chicago, IL 60611, USA
[b]Department of Biomedical Engineering, McCormick School of Engineering, Northwestern University, Evanston, IL 60208, USA
[c]Department of Urologic Surgery, University of California at Davis, Davis, CA 95817, USA
[d]Department of Urology, David Geffen School of Medicine at UCLA, Los Angeles, CA 90095, USA
[e]Biologic Resources Laboratory, University of Illinois at Chicago, Chicago, IL 60612, USA
[f]Department of Urology, University of Illinois at Chicago, Chicago, IL 60612, USA
[g]Flow Cytometry Core, Research Resources Center, University of Illinois at Chicago, Chicago, IL 60612, USA
[h]Department of Urology, Feinberg School of Medicine, Northwestern University, Chicago, IL 60611, USA
[i]Simpson Querrey Institute, Northwestern University, Chicago, IL 60611, USA
[j]Center for Translational Research and Education, Loyola University Chicago, Chicago, IL 60153, USA
[k]Division of Hematology/Oncology, Department of Medicine, University of Illinois Cancer Center, Chicago, IL 60612, USA
[l]Urology San Antonio, San Antonio, TX 78229, USA
[m]Department of Neuroscience, Feinberg School of Medicine, Northwestern University, Chicago, IL 60612, USA
[n]Stanley Manne Children's Research Institute, Louis A. Simpson and Kimberly K. Querrey Biomedical Research Center, Chicago, IL 60611, USA
[o]Center for Advanced Regenerative Engineering, Northwestern University, Evanston, IL 60208, USA
[p]Vascular Surgery, Department of Surgery, Feinberg School of Medicine, Northwestern University, Chicago, IL 60612, USA
*To whom correspondence should be addressed: Email: arun-sharma@northwestern.edu
[1]M.I.B., N.J.F., X.W., Y.Y.C., and R.M.S. contributed equally to this work.
Edited By: Dennis Discher

Abstract

To date, there are no efficacious translational solutions for end-stage urinary bladder dysfunction. Current surgical strategies, including urinary diversion and bladder augmentation enterocystoplasty (BAE), utilize autologous intestinal segments (e.g. ileum) to increase bladder capacity to protect renal function. Considered the standard of care, BAE is fraught with numerous short- and long-term clinical complications. Previous clinical trials employing tissue engineering approaches for bladder tissue regeneration have also been unable to translate bench-top findings into clinical practice. Major obstacles still persist that need to be overcome in order to advance tissue-engineered products into the clinical arena. These include scaffold/bladder incongruencies, the acquisition and utility of appropriate cells for anatomic and physiologic tissue recapitulation, and the choice of an appropriate animal model for testing. In this study, we demonstrate that the elastomeric, bladder biomechanocompatible poly(1,8-octamethylene-citrate-co-octanol) (PRS; synthetic) scaffold coseeded with autologous bone marrow-derived mesenchymal stem cells and $CD34^+$ hematopoietic stem/progenitor cells support robust long-term, functional bladder tissue regeneration within the context of a clinically relevant baboon bladder augmentation model simulating bladder trauma. Partially cystectomized baboons were independently augmented with either autologous ileum or stem-cell-seeded small-intestinal submucosa (SIS; a commercially available biological scaffold) or PRS grafts. Stem-cell synergism promoted functional trilayer bladder tissue regeneration, including whole-graft neurovascularization, in both cell-seeded grafts. However, PRS-augmented animals demonstrated fewer clinical complications and more advantageous tissue characterization metrics compared to ileum and SIS-augmented animals. Two-year study data demonstrate that PRS/stem-cell-seeded grafts drive bladder tissue regeneration and are a suitable alternative to BAE.

Keywords: urinary bladder, regenerative engineering, autologous stem cells, biomechanocompatible scaffold

Competing Interest: A US International Patent has been filed for the poly(1,8-octamethylene-citrate-co-octanol) scaffold through Northwestern University (G.A.A., X.W., M.I.B., and A.K.S.) as it relates to composition of matter and utility. G.A.A. is the inventor of FDA-approved citrate-based biomaterials. The other authors have no competing interests. The NIH may hold certain rights to the intellectual properties described within the patent filing.

Received: July 11, 2023. **Accepted:** January 16, 2024

Significance Statement

Individuals with severe bladder dysfunction have very limited options for bladder tissue replacement. The current standard of care for the end-stage bladder is surgery, where bowel tissue is used as a patch to enlarge the bladder to limit increases in internal bladder pressure. Although this procedure provides limited functional improvement, it is associated with numerous significant short- and long-term complications. Multiple tissue engineering–based studies have failed to provide a clinically translational solution for this problem. Within the context of this study, we describe the utility of a structural, biocompatible scaffold that mimics the physical and mechanical properties of the bladder that was seeded with autologous stem cells, which promoted and maintained long-term bladder tissue regeneration in a large, preclinical animal model.

Introduction

Surgical approaches spanning decades have been utilized to mitigate severe and end-stage urinary bladder dysfunction (1–5). Patients requiring bladder tissue replacement present with acquired (secondary to trauma, spinal cord injury, or malignancy) or congenital disorders (bladder exstrophy). Clinical manifestations of the pathologic bladder can include urinary incontinence, urinary tract infections (UTI), and hydronephrosis (HN) accompanied by renal dysfunction if left untreated or poorly managed. As bladder function gradually deteriorates, surgical intervention is required. Historically, this has relied heavily upon the use of autologous segments of gastrointestinal tissues (small intestine, colon, or stomach) to alternatively serve as a urinary diversion conduit or in a bladder augmentation enterocystoplasty (BAE) setting (6–11). With regards to BAE, the bladder is splayed open or cystectomized, and an autologous, detubularized segment of the bowel (typically the ileum) is grafted onto the defect in an attempt to increase bladder capacity and improve compliance by physically enlarging the bladder (Fig. 1A). However, bladder and ileal tissue are anatomically and physiologically incongruent, presenting numerous postsurgical complications. To date, there is no engineered bladder tissue substitute that is utilized in a clinical setting.

Attempts to create functional bladder tissue replacement products for clinical applications have been met by numerous impediments, leading to insufficient advances in the field (12–16). In order to address the aforementioned challenges, we rigorously examined a multifaceted approach utilizing poly(1,8-octamethylene-citrate-co-octanol) (PRS), a bladder-mechanocompatible, biodegradable scaffold coseeded with bone marrow mesenchymal stem cells (MSCs) and donor-matched bone marrow $CD34^+$ hematopoietic stem/progenitor cells (HSPCs) to achieve long-term functional bladder tissue regeneration in vivo. The impetus to utilize autologous MSCs and $CD34^+$ HSPCs is based on their proregenerative capacity (17–20) coupled with our previous rodent bladder tissue regeneration studies (21, 22). The paracrine nature of the bone marrow MSC secretome has been beneficial in tissue regenerative settings within multiple organ systems (23–25) through actions mediated in part by microvesicles, exosomes, and soluble proteins (26–30). Similarly, $CD34^+$ HSPCs have shown wide proangiogenic activity and contributions to peripheral nerve regeneration (21, 31–33). In our former animal studies (21), MSC/$CD34^+$ HSPC dual-seeded scaffolds proved to be highly efficacious with regard to bladder tissue regeneration compared to single-cell-seeded scaffolds (MSC or $CD34^+$ HSPC alone). The limitations of the rodent model also provided the catalyst to study these cell-seeded composites in a preclinical, large animal model. Within the context of our established baboon bladder augmentation model (34), autologous ileum (E), cell-seeded PRS scaffolds (CS-PRS), or cell-seeded small-intestinal submucosa (SIS; CS-SIS) were grafted onto the partially cystectomized bladder of their original cell donor, resulting in an autologous graft and assessed anatomically and physiologically over 2 years. Our data demonstrate robust bladder tissue regeneration using cell-seeded grafts with regards to bladder smooth muscle and urothelium regeneration accompanied by neurovascular regeneration throughout the entirety of the graft, including its core. Upon physiological evaluation, animals that received CS-SIS and CS-PRS scaffolds were able to perform comparably or better than enterocystoplasty animals within certain regenerative measures without the presence of persistent clinical issues, including mucus overproduction and HN, accompanied by limited detrusor overactivity (DO). We show that the CS-PRS scaffold is superior to autologous ileum enterocystoplasty and CS-SIS, rendering it an innovative biomaterial platform and an attractive clinical alternative for reconstructive surgery for severe bladder dysfunction. Overall, study data demonstrate that our grafted composites can be successfully utilized to regenerate bladder tissue within the context of an animal model that is anatomically and physiologically similar to human counterparts.

Results

Longitudinal bladder clinical evaluations and capacity assessment

To evaluate the utility of the CS-PRS construct with regards to bladder capacity recovery associated with minimal complications, clinical assessments of CS-PRS and control groups (CS-SIS, E) were conducted at an early recovery stage (6 weeks) and at 6-month intervals (6/12/18/24 months) after partial cystectomy (~50–65% reduction of native bladder) and augmentation. During assessments, animals were evaluated for the development of HN, DO, urine leakage (UL), hydroureter (HU), vesicoureteral reflux (VUR), and mucus production (MP). Capacity recovery was assessed as a percentage of the initial (precystectomy) measurement (100% recovery indicating augmented bladder at the same capacity as native bladder precystectomy). Fluoroscopy imaging, cystometry tracings, bladder ultrasound, and kidney ultrasound ± Doppler were utilized for bladder physiological measurements and observations (Fig. 1B–D; all animals in Figs. S1–S3). UTIs were tracked throughout the study (Table S1). Animals are indicated by either M (male) or F (female) followed by a unique identification number.

Before the 6-week mark, postprocedure UTIs were detected in 3/14 animals (E 2/5, F54 7 days and M50 24 days post; CS-SIS 1/5, F19 35 days post; CS-PRS 0/4). At the early recovery stage (6 weeks), 6/14 animals were assessed with new HN, DO, and/or UL (E 3/5, CS-SIS 1/5, CS-PRS 2/4) (Fig. 2A). In the E group, both HN and DO were noted in 2/5 animals (M50 [also pre-6 weeks UTI], F52 [also 6 week UL]), and DO alone was observed in 1/5 (F54 [also pre-6 week UTI]). One CS-SIS animal was noted for DO/UL at 6 weeks (1/5; F16). In the CS-PRS group, HN, DO, and UL were observed

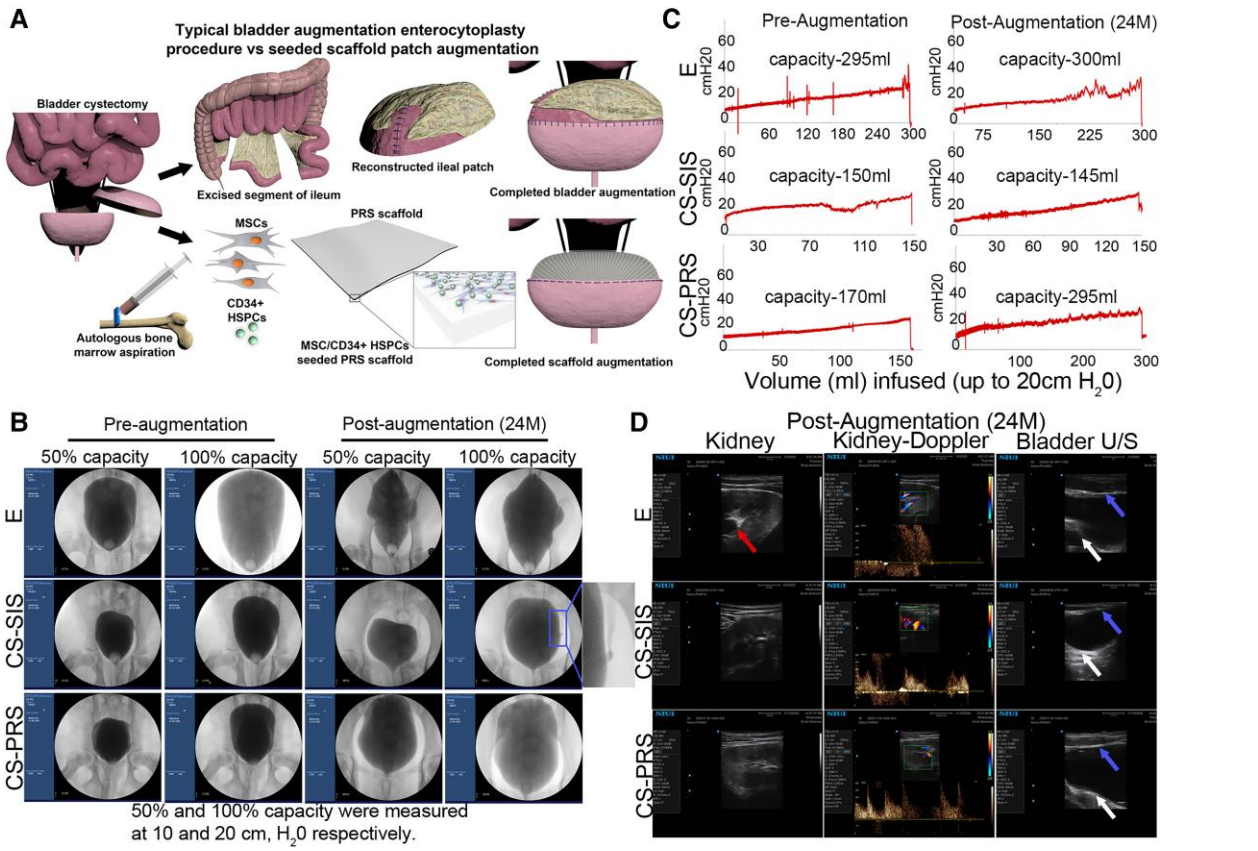

Fig. 1. Longitudinal bladder capacity assessment. A) Graphical depiction of bladder augmentation enterocystoplasty (BAE; E group) that utilizes autologous ileum as a pseudo-bladder replacement (top panel). This procedure gives rise to numerous complications. The bottom panel depicts augmentation with a cell-seeded scaffold (MSCs and $CD34^+$ HSPCs seeded onto a PRS scaffold). B) Sample study fluoroscopy images immediately preaugmentation and 24 months postaugmentation (images for all animals, Fig. S1; E F54, CS-SIS M24, CS-PRS M27 shown here). All 100% capacity images are at an intravesical pressure of 20 cm H_2O; studies stopped at this point to decrease the risk of iatrogenic bladder perforation. Imaging was utilized in the evaluation for VUR and to assess bladder contour at 6 weeks and 6/12/18/24 months. VUR was identified in 1/14 animals across study time points (CS-SIS M24, middle row, columns III–IV). Irregular bladder shape is visible at 50% capacity at 24 months postaugmentation in E and CS-SIS groups. As SIS lacks proper rigidity that is comparable to native baboon (as well as human) bladder tissue, this is not an unexpected result. Decreased mean solidity (a measure of boundary regularity) was also observed for E (50 and 100% capacity) and CS-SIS (50% capacity) groups, but not for the CS-PRS group (for each group, preprocedure solidity levels vs. 24-month postaugmentation solidity levels; Fig. S1). C) Sample study cystometry tracings (fill rate 10% bladder capacity/min) immediately presurgical procedure and 24 months postaugmentation (images for all animals, Fig. S2; E F54, CS-SIS M24, CS-PRS M27 shown here). Capacity (mL) at 20 cm H_2O listed within tracings. Capacity (mL and percent recovery) shown in Fig. 2A–D and Table S2; 24 months percent recovery E F54 101.7% (E group 38.2–491.9%), CS-SIS M24 96.7% (CS-SIS group 47.3–96.7%), and CS-PRS M27 173.5% (CS-PRS group 63.6–173.5%). At 24 m, DO was observed in E 54 (first row, column II). In 6/12/18/24-month assessments, DO was observed in 5/5 E animals (1–3 time points), 2/5 CS-SIS animals (single time point), and 1/4 CS-PRS animals (single time point) (Fig. 2A); all time points for each animal Table S1). D) Sample study renal ultrasound and Doppler images (first two columns) and bladder ultrasound images (third column) at 24 months postaugmentation (images for all animals, Fig. S3; E M50, CS-SIS F16, CS-PRS F21 shown here). At 24 months, HN (red arrow) was detected in E M50 (first row). This animal was also notable for an extreme rise in capacity. In 6/12/18/24 m assessments, HN was detected in 2/5 E animals (no CS-SIS or CS-PRS animals) (Fig. 2A; all time points for each animal Table S1). White arrows = native bladder tissue and blue arrows = ileal or regenerated bladder tissue.

for one animal at 6 weeks (1/4; F20) and DO alone for another (1/4; M26). In subsequent (6–24 months) assessments of animals with 6 weeks HN, DO, and/or UL, HN was observed again only for E M50 (persistent at 12/18/24 months), and UL was only noted again for E F52 (12 months). Both E M50 (pre-6-week UTI, 6-week HN/DO) and F52 (6-week HN/detrusor overactivity/UL) showed capacity recovery that differed from the rest of the E group. M50 demonstrated extreme capacity (24 months 491.9%) and F52 exhibited multiple instances of capacity decrease, with a 24-month recovery <50%. DO was observed again for all three E animals (1–3 time points) and for CS-SIS F16 (one time point). MP, observed for all E animals at 6 weeks, continued to be noted throughout the study for the E group (Table S1).

During the 6- to 24-month recovery phase (clinical evaluations at 6/12/18/24 months), DO was observed with varying frequency across groups (E 5/5; CS-SIS 2/5; CS-PRS 1/4), HN and urine leak were only detected in E animals (HN 2/5; urine leak 1/5), VUR was only identified in a CS-SIS animal (1/5), and no HU was noted (HN/DO/urine leak/VUR/HU 6–24 months: 9/14 animals [E 5/5, CS-SIS 3/5, CS-PRS 1/4; 3/6 months and 6/8F]) (Fig. 2A). Across 6-month interval clinical evaluations, persistent DO (4/5) or HN (1/5) was noted for E animals. DO was detected at 2–3 time points (50–75% of evaluations) for 4/5 animals. For two of these animals, urine leak/UTI or HN was also noted during the 6- to 24-month recovery stage (M57 12/18 months DO; F52 6/12/18 months DO + 12 months urine leak + 12–18 months UTI; F54 6/18/24 months DO; F56 6/12 months DO + 18 months HN). Persistent HN was observed for E M50 (6 weeks HN/DO; 12 months HN, 18 months HN/DO, 24 months HN; also noted for extreme capacity [described below]). Urine leak, observed at 6 weeks for E F52, was detected again

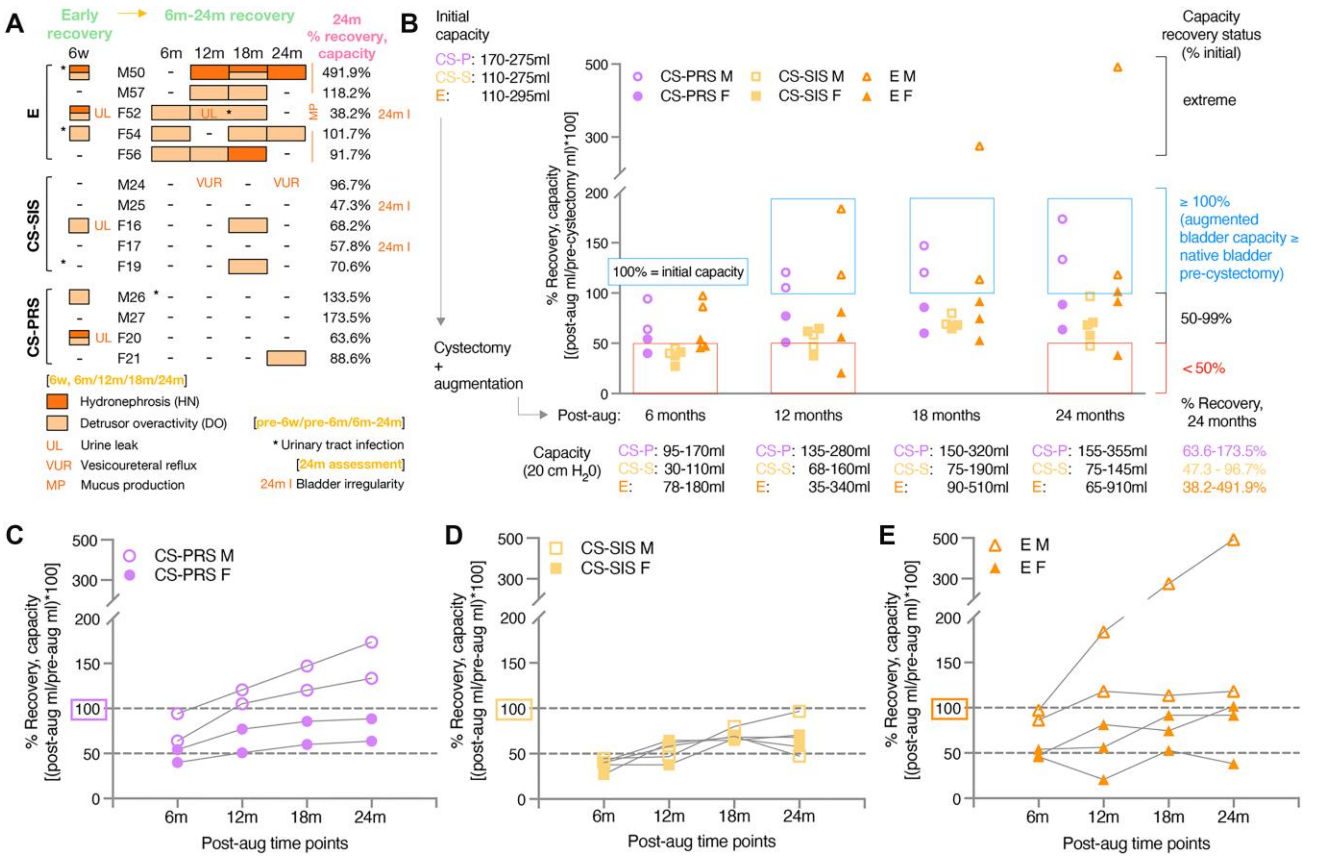

Fig. 2. Bladder capacity and physiological assessment. A) At each postaugmentation time point (6 weeks, 6/12/18/24 months), animals were evaluated for the development of HN (dark orange boxes), DO (light orange boxes), UL (orange text), HU (no instances detected), VUR (orange text), and MP (orange text) (Table S1). UTIs (asterisks), CBC (complete blood count), blood biochemistry, and urinalyses were tracked throughout the study (Table S1 [UTIs, pre-6w, pre-6, and 6–24 m]; Data File S1). At the early recovery stage (6 weeks; far left column), 6/14 animals were assessed with HN, DO, and/or UL (2M [2/6M] and 4F [4/8F]; E 3/5, CS-SIS 1/5, CS-PRS 2/4). HN and DO were observed in 3/14 animals, two with UL (E 2/5 and CS-PRS 1/4). DO alone or with UL was noted in an additional 3/14 animals (E 1/5, CS-SIS 1/5, CS-PRS 1/4). Dash indicates not observed. Pre-6w and pre-6m UTIs are designated with asterisks. For each animal, male (M) or female (F) and unique number identifier is listed. E $n = 5$ animals (2M/3F); CS-SIS $n = 5$ animals (2M/3F); CS-PRS $n = 4$ animals (2M/2F). In the 6- to 24-month recovery phase (time points: 6/12/18/24 m), HN was detected in 2/5 E animals (no CS-SIS or CS-PRS animals) and DO was observed in 5/5 E animals (1–3 time points), 2/5 CS-SIS animals (single time point), and 1/4 CS-PRS animals (single time point). VUR was identified in one CS-SIS animal (two time points). UL and UTI were noted in one E animal (F52; UTI detected between 12 and 18 months, UL/DO/presence of blood in mucus at 12 months). MP was detected for all E animals across time points (E animals only). No HU was observed. At the 24 months assessment, specific bladder irregularities were noted for three animals (denoted as 24 months I, far right; E 1/5 [irregular filling] and CS-SIS 2/5 [diverticulum, dome irregularity]). B) Initial (precystectomy) native bladder capacity (mL) ranged from 110 to 295 across the three groups (group ranges upper left; F 110–295 and M 110–275; all capacity measurements at 20 cm H_2O; individual values, Table S2). Partial cystectomy reduced native bladder by ~50–65% (estimates of native capacity postprocedure listed in Table S2) and was followed by augmentation with an ileal graft or cell-seeded scaffold (Video S1; augmentation surgery of CS-PRS). Postaugmentation capacity measurements (mL; range for each group listed below each time point; individual values, Table S2) occurred at 6 weeks (early recovery stage), and at 6-month intervals from 6 to 24 months (6/12/18/24 months). To determine % recovery, each measurement was divided by initial precystectomy capacity ([postaugmentation mL/initial precystectomy mL] × 100). Values ≥100% indicated recovery of the augmented bladder to the precystectomy level and further increase in capacity. Right brackets denote extreme, ≥ 100, 50–99, and <50% recovery levels; blue and red boxes indicate the ≥100 and <50% recovery zones. Note that the y-axis has two segments to accommodate the extreme increase E animal (B–E). At 24 months, 1/5 E animals were notable for extreme capacity (1M), 2/5 E (1M/1F), and 2/4 CS-PRS (2M) animals showed progression to ≥100% recovery, and an additional two animals reached ≥90% (1 E [F] and 1 CS-SIS [M]). Two animals were below the 50% recovery threshold (1/5 E [F] and 1/5 CS-SIS [M]). Range of % recovery for each group at 24 months listed lower right (24 months values for each animal, [A] [right column]; all values, Table S2). C–E) Trajectories of capacity recovery (6–24 months) shown for each animal of each group ($n = 4$–5). The four CS-PRS animals C) showed gradual 6- to 18-month increases, with 18- to 24-month flattening for F and continued increase for M. Trajectory for the CS-SIS group (D) was variable (3/5; 1M, 2F) or variable with an 18- to 24-month decrease (2/5; 1M 24 months 47.3%, 1F 24 months 57.8%). In the E group (E), 3/5 animals (1M, 2F) were variable in recovery (periods of increase, plateau, slight increase/decrease), 1/5 (M) showed an extreme rise to 491.9% and 1/5 (F) decreased twice, with 24 months recovery <50% (38.2%). B–E) CS-PRS ($n = 4$; 2M/2F) purple circles or text; CS-SIS ($n = 5$; 2M/3F) yellow squares or text; E ($n = 5$; 2M/3F) orange triangles or text. For all groups, open symbol M and filled symbol F.

(12 months urine leak and presence of blood in urine mucus and in the urine, decrease in capacity), along with multiple instances of DO (6 weeks HN/DO/urine leak; 6 months DO, 12 months DO/urine leak, 18 months DO), detection of a UTI in the 12- to 18-month time period, and decreases in capacity (6–12 and 18–24 months), resulting in the lowest 24-month capacity recovery across animals (38.2%). In the CS-SIS group, VUR was identified in 1/5 animals (M24 12/24 months), and DO was observed at a single time point for 2/5 (F16 and F19 18 months). For CS-PRS animals, one animal was noted for DO at a single time point (F21 24 months). In the 6- to 24-month stage, UTI was detected in 1/14 animals (E F52; described above), with an additional detection (CS-PRS M26) after the early recovery stage (6 weeks) but before the 6- to 24-month stage (Table S1). As would be expected, irregularities in the bladder wall and mucosa were observed in the E group, with MP in all E animals at each time point. At the

24-month assessment, irregular bladder shape was apparent in fluoroscopy imaging at 50% capacity levels for E and CS-SIS animals. Further 24-month deviations included irregular filling (E F52), bladder diverticulum (CS-SIS M25), and bladder dome irregularity (CS-SIS F17) (Fig. S1). In combination, detection of HN/DO/urine leak/VUR at any 6- to 24-month time point and/or 24-month specific irregularities occurred for 5/5 E animals, 5/5 CS-SIS animals, and 1/4 CS-PRS animals (Table S1).

Bladder capacity recovery

Recovery of capacity was tracked from 6 to 24 months, with % recovery levels used to evaluate stages of improvement (each measurement as a percentage of the initial precystectomy value; 100% recovery indicating augmented bladder at the same capacity as native bladder precystectomy) (Fig. 2B; Table S2). At 6 months, 3/4 CS-PRS and 3/5 E animals achieved ≥50% recovery, with the remaining animals in these two groups at ≥40% (6 months CS-PRS 40.0–94.1%; 6 months E 45.9–97.3%). None of the CS-SIS animals were yet at the ≥50% stage (6 months CS-SIS, 27.3–44.7%). CS-SIS progression continued to be limited, comparatively, with no animals ≥100% at any time point (by 12 months, 2/4 CS-PRS and 2/5 E animals ≥100%). The trajectory of recovery from 6 to 24 months varied across and, in some cases, within groups (Fig. 2C–E). All four CS-PRS animals showed a continued, gradual increase in recovery from 6 to 18 months, with a sharper overall rise and continued 18- to 24-month increase observed for M, and an 18- to 24-month flattening for F (CS-PRS 24-month recovery status: 0/4 extreme; 2/4 ≥ 100% [M26/M27, 133.5–173.5%]; 2/4 50–99% [F20/F21, 63.6–88.6%]; 0/4 < 50%; Fig. 2C). Both the E and CS-SIS groups showed a mix of trends, including decreases in capacity (Fig. 2D and E). In the E group, 3/5 animals were variable in recovery (periods of increase, plateau, slight increase/decrease), 1/5 showed an extreme rise over time (97.3%/183.8%/275.7%/491.9%), and 1/5 showed two instances of decrease, at the 6- to 12-month interval (45.9 to 20.6%) and again at 18–24 months (52.9 to 38.2%, resulting in 24-month recovery <50%) (E 24 month recovery status: 1/5 extreme [M50, 491.9%]; 2/5 ≥ 100% [M57/F54, 101.7–118.2%]; 1/5 50–99% [F56, 91.7%]; 1/5 < 50% [F52, 38.2%]). Clinical evaluation observations for the E extreme and low-capacity animals are described above. In the CS-SIS group, 3/5 animals were variable in recovery trajectory, and 2/5 were variable with a decrease at the 18- to 24-month interval (resulting in a 24-month recovery level of <50% (47.3%) for M25, and of 57.8% for F17). None of the CS-SIS animals progressed to ≥100% recovery by 24 months (CS-SIS 24-month recovery status: 0/5 extreme; 0/5 ≥ 100%; 4/5 50–99% [M24, 96.7% and F16/F17/F19, 57.8–70.6%]; 1/5 < 50% [M25, 47.3%]). For animals with 18- to 24-month decreases (E, CS-SIS), fluoroscopy revealed irregular filling (E F52), bladder diverticulum (CS-SIS M25), or bladder dome irregularity (CS-SIS F17) at 24 months (Table S1). Throughout the study, the highest levels of capacity recovery were observed in male animals (24 months ≥100% recovery [or extreme capacity]: 4/6 months [CS-PRS, E], and 1/8F [E]). Overall, at 24 months, the capacity range was 155–355 mL for CS-PRS (precystectomy 170–275 mL), 65–910 mL for E (precystectomy 110–295 mL), and 75–145 mL for CS-SIS (precystectomy 110–275 mL) (Table S2).

By 24 months, different profiles had emerged for the three groups. The CS-PRS group was characterized by both the absence of complications and clinical observations suggestive of possible bladder instability, as well as by the gradual progression of capacity recovery (steady increase through 18 months, with continued 18- to 24-month rise for M and flattening for F). Across the four 6- to 24-month clinical evaluations, DO was detected for one CS-PRS animal at a single time point (F21, 24 months); no other animals in this group were noted for any HN/DO/urine leak/VUR/HU in the 6- to 24-month period. Recovery status at 24 months was ≥100% (indicating a level of capacity at or beyond native bladder precystectomy) for 2/4 animals (2M, 133.5–173.5%), and 50–99% for 2/4 (2F, 63.6–88.6%), with no extreme or <50% recovery animals in this group. In the E group, 6- to 24-month evaluations indicated persistent DO or HN for all animals, and capacity recovery was mixed (24 months 38.2–491.9%) and variable in trajectory. DO was observed at two to three 6- to 24-month time points (50–75% of evaluations) for 4/5 E animals; two of these animals were further noted for HN or urine leak/UTI. HN was detected at three 6- to 24-month time points (75% of evaluations) for 1/5 animals. MP was noted throughout the study (5/5 E animals). Recovery progression levels at 24 months included extreme (1/5, 491.9%), ≥ 100% (2/5, 101.7–118.2%), 50–99% (1/5, 91.7%), and <50% (1/5, 38.2% after multiple decreases). The CS-SIS group was noted for bladder irregularities and overall lower levels of capacity recovery progression, with 18- to 24-month capacity decreases for 2/5 animals. Clinical observations for the CS-SIS group included DO (2/5, one time point) and VUR (1/5, two time points [M24, highest CS-SIS 24-month capacity animal]). Specific irregularities (diverticulum, bladder dome irregularity) were detected at 24 months for both 18- to 24-month capacity decrease animals. At 6 months, none of the CS-SIS animals had reached 50% recovery (6-month CS-SIS 27.3–44.7%, vs. CS-PRS 40.0–94.1% and E 45.9–97.3%). By 24 months, recovery was <50% for 1/5 (1M) and 50–99% for 4/5 (1M 96.7%, 3F 57.8–70.6%), with no animals in this group progressing to ≥100%.

Quantitative measurements of regenerated bladder tissue

Bladder tissue smooth muscle quantification

In an assessment of muscle and collagen, where each was considered as a percentage of the combined total, native bladder tissue (Fig. 3A) was split between muscle and collagen, with an overall range of 41.8–61.4% muscle (% muscle: CS-PRS 50.5 ± 1.4 [46.7–53.2]; CS-SIS 47.4 ± 1.6 [43.2–52.1]; E 52.4 ± 3.2 [41.8–61.4]). This native bladder range for muscle and collagen levels was observed for regenerating tissue in CS-PRS animals (% muscle: CS-PRS 50.6 ± 2.7 [45.2–55.7]), while regenerating tissue in CS-SIS animals showed a greater proportion of collagen at this time point (% muscle: CS-SIS 36.5 ± 2.7 [31.3–44.8]; CS-PRS vs. CS-SIS, $P < 0.01$) (Fig. 3B). As a different tissue type, E ileal grafts were found to be outside the native bladder range and weighted more heavily toward muscle (E 85.2 ± 1.2 [81.4–88.6]; E vs. CS-PRS and CS-SIS, $P < 0.0001$).

Animals with muscle levels <40% (CS-SIS 3/5 [60%], 2F and 1M) were observed to have the lowest within-group levels of capacity recovery at 24 months (CS-SIS, <40% muscle [2F/1M, 31.1–33.2%]: 24-month capacity recovery 47.3–68.2% vs. >40% muscle [1F/1M, 41.1–44.8%]: 24-month capacity recovery 70.6–96.7%). Two of the low-muscle/high-collagen animals (1M, 1F) were among the 3/14 animals with a decrease in capacity at the 18- to 24-month interval (F17 66.7 to 57.8% and M25 69.1 to 47.3%; described in the previous section). At higher levels of % muscle (>45%), either a narrower, elevated range was detected, with no apparent correspondence to capacity (E), or differences in capacity recovery and possibly % muscle appeared more likely to be related to M/F differences (CS-PRS, M % muscle 45.2–46.9 and 24-month capacity recovery 133.5–173.5%; F % muscle 54.7–55.7

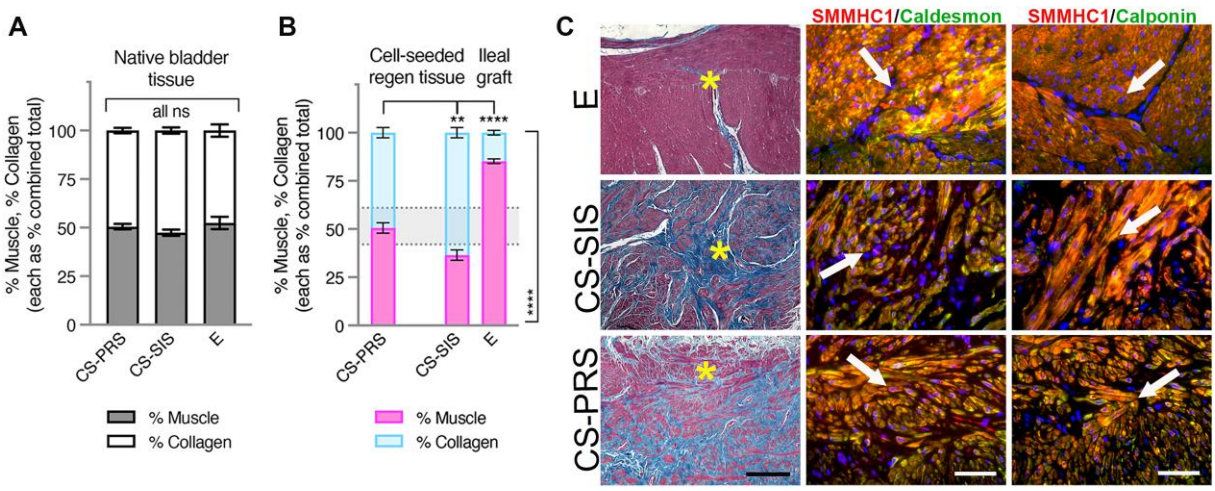

Fig. 3. Bladder tissue smooth muscle quantification. A) Muscle/collagen levels for native bladder tissue (shown as stacked bars, each as percentage of combined total [% muscle, gray, bottom bar and % collagen, white, top bar]) were comparable across groups, with an overall range (all animals) of 41.8–61.4% muscle depicted in (B) with dotted lines. B) For CS regenerating tissue and E ileal grafts, muscle/collagen levels (stacked bars, each as percentage of combined total [% muscle, pink, bottom bar and % collagen, blue, top bar]) are shown with dotted lines marking native bladder tissue range. Regenerating tissue in CS-PRS animals was within this range (% muscle: 50.6 ± 2.7 [45.2–55.7]), while regenerating tissue in CS-SIS animals showed a greater proportion of collagen (% muscle: 36.5 ± 2.7 [31.3–44.8]; CS-SIS vs. CS-PRS $^{**}P < 0.01$ [top bracket]). E ileal grafts were outside the range and weighted toward muscle (% muscle: 85.2 ± 1.2 [81.4–88.6]; E vs. CS-PRS and vs. CS-SIS, $^{****}P < 0.0001$ [top and side brackets]). A and B) Data presented as mean ± SEM; $n = 4$–5 animals/group. All ns (A) indicate no statistically significant difference for any group comparison (CS-PRS vs. CS-SIS, CS-PRS vs. E, E vs. CS-SIS). Statistical significance ($^{**}P < 0.01$, $^{****}P < 0.0001$, ns = not significant) determined by one-way ANOVA with Tukey–Kramer post hoc test ($P < 0.05$ considered statistically significant). CS-PRS $n = 4$ animals (2M/2F); CS-SIS $n = 5$ animals (2M/3F); E $n = 5$ animals (2M/3F). C) Column I: Tissue from E ileal grafts demonstrated an overabundance of smooth muscle (red) derived directly from the musculature of the grafted ileum as demonstrated by Trichrome staining. The lack of oriented muscle fascicles combined with the relatively low abundance of collagen (blue) family members can lead to noncontractile bladder tissue. CS-PRS and CS-SIS groups demonstrated mean levels of ~50 and ~36% muscle, respectively, reflecting significantly higher mean muscle content in CS-PRS grafts compared to CS-SIS grafts. ~1:1 muscle/collagen ratio is considered normal distribution as demonstrated in (A) and corroborated by other studies across multiple species (35). Columns II and III demonstrate immunofluorescence (IF) costaining of the regenerated region of ileal or cell-seeded grafted areas with regards to bladder tissue smooth muscle. Tissues were co-immunostained with antibodies against smooth muscle myosin heavy chain (SMMHC) and either caldesmon or calponin. The latter two proteins are pivotal in smooth muscle cell contraction and overall coordinated bladder micturition cycles. Images are representative of multiple samples/animals within a group at study termination. Yellow asterisks denote the area in which the IF images were taken while white arrows demonstrate colocalization of the aforementioned muscle markers. Blue, DAPI. Magnification-Trichrome 100× and IF 400× (scale bar, Trichrome 250 μm and IF 50 μm). Tissue-centric analyses utilized samples at 24 m (CS-PRS); 24 m (one animal at 27 m, E); 26–29 m (CS-SIS).

and 24-month capacity recovery 63.6–88.6%; group size [2F/2M] limits consideration of CS-PRS M/F % muscle potential trend, as M/F differences in % muscle were not observed more widely). Tissue underwent Trichrome and IF staining with bladder smooth muscle markers followed by quantitative morphometrics (Fig. 3C; all animals in Fig. S4).

Bladder tissue vascularization quantification

E ileal grafts showed a different vasculature profile than CS scaffolds, with a comparable number of larger (>2,500 μm^2) vessels/mm^2 (CS-PRS 1.2 ± 0.2 [1.0–1.8]; CS-SIS 0.9 ± 0.2 [0.1–1.5]; E 1.2 ± 0.4 [0.6–2.6]), but significantly fewer smaller (≤2,500 μm^2) vessels/mm^2 (CS-PRS 17.1 ± 1.4 [13.1–19.5] and CS-SIS 15.9 ± 2.3 [8.5–20.9] vs. E 7.1 ± 0.8 [4.3–8.6]; $P < 0.01$; Fig. 4A). In comparison to native bladder tissue, all three groups displayed a moderate downward shift in the number of larger vessels (group means 0.7× native) (NATIVE: CS-PRS 1.7 ± 0.5 [0.6–2.9]; CS-SIS 1.3 ± 0.2 [0.9–2.2]; E 1.8 ± 0.2 [1.4–2.4]), with differing CS and E trends observed for smaller vessels (Fig. 4A and B). CS scaffolds showed an upward expansion of the range observed for native bladder tissue (1.3–1.4×), while E ileal grafts were below that range (0.6×) (NATIVE: CS-PRS 13.6 ± 1.1 [10.7–16.0]; CS-SIS 11.6 ± 1.7 [6.8–16.4]; E 12.1 ± 0.6 [10.3–13.7]). The reduced number of smaller vessels in E ileal grafts did not translate to a significant difference in mean percent vasculature (PV; CS-PRS 1.70 ± 0.06 [1.53–1.81]; CS-SIS 1.37 ± 0.10 [1.15–1.74]; E 1.27 ± 0.25 [0.59–2.07]), although the E group was notable for the lowest individual animal PV values, and the widest range for REGEN groups (Fig. 4C). Mean PV for regenerating and graft tissue overlapped in range with native tissue but did not include as many individual values >2% (NATIVE: CS-PRS 1.91 ± 0.31 [1.14–2.63]; CS-SIS 1.51 ± 0.13 [1.22–1.85]; E 1.98 ± 0.14 [1.65–2.35]; Fig. 4C and D). Further evaluation of PV indicated heightened levels of vasculature for CS-PRS animals. Mean PV was ≥1.5% for all CS-PRS animals, whereas fewer CS-SIS and E animals reached this level (≥1.5%: CS-PRS 4/4, CS-SIS 1/5, E 2/5). Additionally, assessment of minimum and maximum vasculature levels for each animal revealed elevated minimum vasculature values for the CS-PRS group. Levels were significantly higher than CS-SIS and E, and appeared to display an upshift from native bladder tissue (CS-PRS 0.73 ± 0.07 [0.60–0.86] vs. CS-SIS 0.33 ± 0.10 [0.09–0.66], $P < 0.05$; vs. E 0.17 ± 0.10 [0.00–0.55], $P < 0.01$; NATIVE: CS-PRS 0.25 ± 0.06 [0.12–0.36]; CS-SIS 0.39 ± 0.05 [0.26–0.55]; E 0.38 ± 0.13 [0.06–0.69]; Fig. 4E and F). Max values showed an overlapping range for the three groups (REGEN: CS-PRS 3.54 ± 0.21 [2.94–3.84]; CS-SIS 3.15 ± 0.32 [2.51–4.22]; E 3.93 ± 0.93 [2.13–7.02] and NATIVE: CS-PRS 4.69 ± 0.63 [3.10–6.15]; CS-SIS 4.01 ± 0.60 [2.56–5.81]; E 4.36 ± 0.20 [3.96–5.08]; Fig. 4G and H). Trichrome staining corroborated vascular quantification measurement data in grafted areas. Dual vWF/CD31 IF staining demonstrated blood vessels present throughout the entirety of the grafted area with a similar distribution of vessels amongst all groups postaugmentation (Fig. 4I; all animals in Fig. S5).

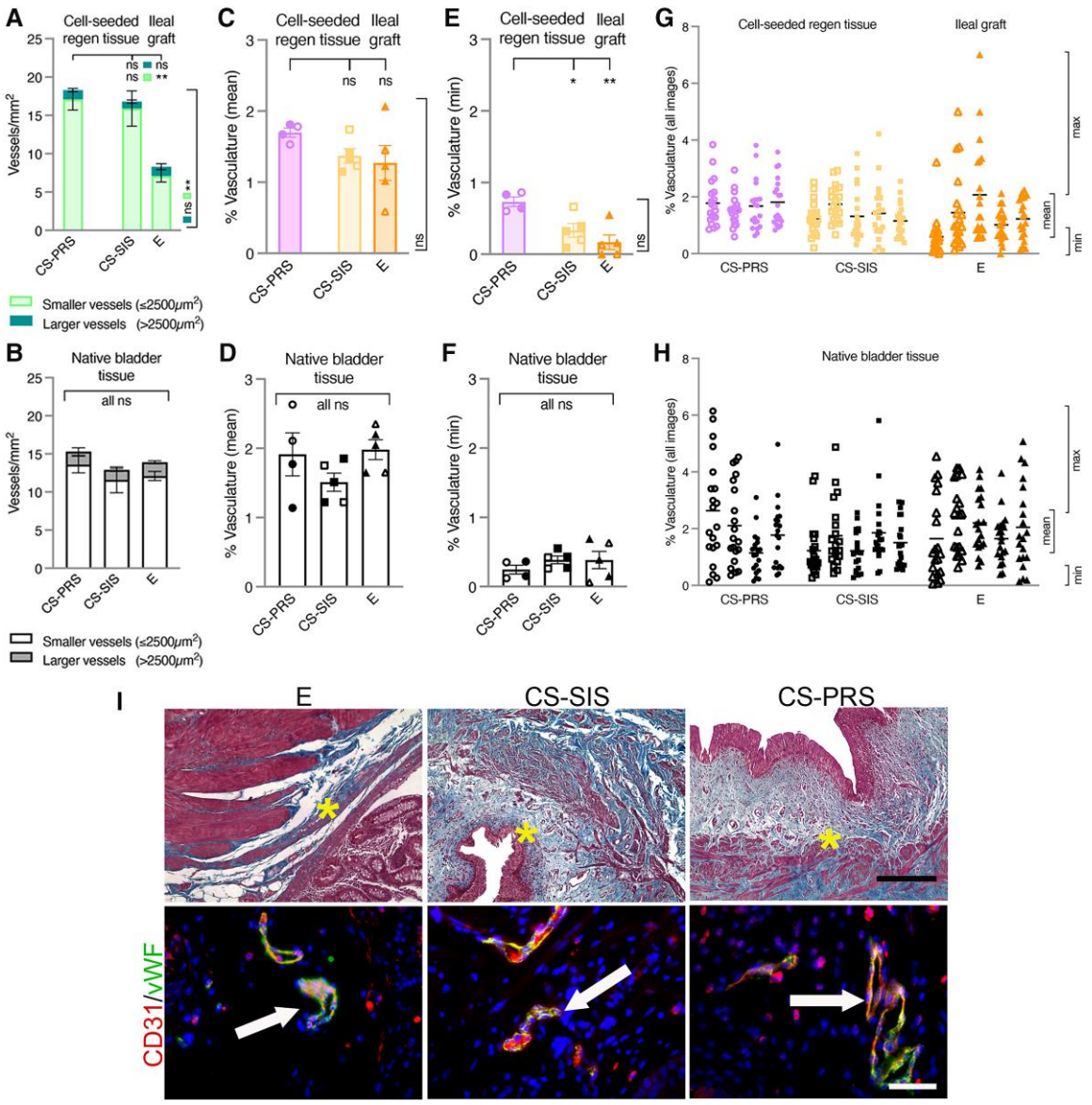

Fig. 4. Bladder tissue vascularization assessment. A and B) Vessels were classified as smaller (≤2,500 μm^2) or larger (>2,500 μm^2) for expanded characterization of vasculature. A) CS scaffolds and E ileal grafts differed in their vasculature profiles, with comparable numbers of larger vessels/mm^2 (darker green, top bars in stack), but significantly fewer smaller vessels/mm^2 (lighter green, bottom bars in stack) for E animals (CS-PRS and CS-SIS vs. E, $^{**}P < 0.01$ [top and side brackets]). B) In native bladder tissue, numbers of smaller (white, bottom bars in stack) and larger (gray, top bars in stack) vessels/mm^2 were similar across groups (all group comparisons ns). C–H) PV was evaluated across images (20 images/animal) for trends in mean, minimum, and maximum levels. C) Mean PV was not significantly different across the CS scaffold and E ileal graft groups (ns, top and side brackets). A wider range of values was observed for the E group, while the CS-PRS group was noted for a greater number of values ≥1.5% (≥1.5%: CS-PRS 4/4, CS-SIS 1/5, E 2/5). D) Native bladder tissue vasculature levels (here as mean PV) were similar across groups (all group comparisons ns). E) A significant upshift in minimum PV values was observed for CS-PRS animals (CS-PRS vs. CS-SIS $^{*}P < 0.05$ and CS-PRS vs. E $^{**}P < 0.01$ [top bracket]) (Group differences in min PV also apparent in [G]). F) Native bladder tissue vasculature levels (here as min PV) were similar across groups (all group comparisons ns). G–H) Data points representing each image for each animal shown (20 images/animal), with horizontal lines marking mean values for each animal, and ranges for mean, minimum, and maximum PV bracketed on the right. G) Max PV values overlapped in range across CS scaffold and E ileal graft groups (CS-PRS 3.54 ± 0.21 [2.94–3.84]; CS-SIS 3.15 ± 0.32 [2.51–4.22]; E 3.93 ± 0.93 [2.13–7.02]). H) Native bladder tissue vasculature levels (mean/min/max PV) were similar across groups. A–F) Data presented as mean ± SEM. C–F) Individual data points for each animal are overlaid on corresponding bars. All ns (B, D, F) indicate no statistically significant difference for any group comparison (CS-PRS vs. CS-SIS, CS-PRS vs. E, E vs. CS-SIS). Statistical significance ($^{*}P < 0.05$, $^{**}P < 0.01$, ns = not significant) determined by one-way ANOVA with Tukey–Kramer post hoc test. CS-PRS (circles) $n = 4$ animals (2M/2F); CS-SIS (squares) $n = 5$ animals (2M/3F); E (triangles) $n = 5$ animals (2M/3F). All groups, open symbols M and filled symbols F. I) Trichrome staining demonstrated the presence of blood vessels throughout the entirety of the grafted areas of the three experimental groups. This was corroborated with IF staining using vWF with CD31. The resulting colocalized staining (white arrows) was yellow/orange in color and was indicative of tissue vascularization via vasculogenesis or angiogenesis pathways. There was no evidence of necrotic bladder tissue at study termination or patchy tissue vascularization in any group. Images are representative of multiple samples/animals within a group at study termination. Yellow asterisks represent the area in which the IF images were taken. Blue, DAPI. Magnification-trichrome 100× and IF 400× (scale bar, trichrome 250 μm and IF 50 μm).

Bladder tissue peripheral nerve innervation

Positive βIII-tubulin (neuronal element marker) staining was detected in CS scaffold regenerating tissue and in E ileal grafts, with comparable βIII-tubulin(+) nerve mean area (μm^2) across groups (REGEN: CS-PRS 504.5 ± 54.8 [396.8–638.3]; CS-SIS 451.7 ± 21.8 [403.6–518.9]; E 485.9 ± 17.3 [452.5–552.6]) as well as a similar downshift (~0.5×) from native bladder nerve mean area (NATIVE: CS-PRS 1019.6 ± 27.3 [966.1–1067.4]; CS-SIS 990.1 ± 43.8 [872.5–1142.2]; E 959.7 ± 43.4 [849.1–1114.5]; Fig. 5A). Both the indication of innervation in graft and regenerating tissue and the level of downshift from native bladder tissue correspond to the trends observed in contractile response after stimulation of nerve fibers (high-frequency stimulation of bladder strips, described in the Electrophysiological assessment of bladder tissue section). Trichrome and dual βIII-tubulin/synaptophysin IF staining demonstrated the presence of peripheral nerve formation in all groups throughout the entirety of the grafted area postaugmentation (Fig. 5B; all animals in Fig. S6).

Bladder tissue urothelium/epithelium width quantification and bladder tissue thickness

Mean urothelium width (μm) for the regenerating tissue in CS scaffold animals was within or approaching the range for native bladder tissue (NATIVE: CS-PRS 62.8 ± 3.2 [55.5–69.3]; CS-SIS 60.5 ± 4.9 [48.3–76.7]; E 61.4 ± 6.8 [45.5–78.5] and REGEN: CS-PRS 68.7 ± 3.7 [60.1–78.2]; CS-SIS 52.9 ± 6.1 [41.2–75.3]). Reduced mean epithelium width (μm) in E ileal grafts reflected the different tissue type (E 41.1 ± 2.0 [35.1–46.1]; vs. CS-PRS $P < 0.01$, vs. CS-SIS n.s.; Fig. 6A and B) graft or regenerating tissue thickness (mm) was below the range of native bladder for all three groups (NATIVE: CS-PRS 6.0 ± 0.1 [5.9–6.1]; CS-SIS 5.7 ± 0.1 [5.4–5.9]; E 5.8 ± 0.1 [5.5–6.2] and REGEN: CS-PRS 3.2 ± 0.2 [3.0–3.7]; CS-SIS 3.3 ± 0.1 [3.2–3.4]; E 2.5 ± 0.1 [2.3–2.7]), with the lowest values observed for E animals (E vs. CS-PRS and CS-SIS, $P < 0.001$; Fig. 6C and D). Trichrome and dual pancytokeratin/UPIII (uroplakin III) IF staining demonstrated the presence of water-tight urothelium/epithelial regeneration. The spatial orientation of regenerated urothelium in the CS-SIS and CS-PRS groups resembled native urothelium architecture compared to the E group ileal epithelium (Fig. 6E; all animals in Fig. S7).

Electrophysiological assessment of bladder tissue

The responses in CS regenerating tissue and E grafts were consistent with smooth muscle contractile function and neural innervation. All groups showed responses that had not yet reached the level of native bladder tissue (Fig. 7A–C).

Tissue transcriptome analysis

High-throughput next-generation mRNA sequencing studies were undertaken to analyze the cell transcriptome profile by comparing native to augmented bladder tissues at study termination. For the E, CS-SIS, and CS-PRS groups ($n = 5$, $n = 5$, $n = 4$, respectively), analyses revealed 890, 39, and 47 unique genes significant at the 0.005 level of the univariate test, respectively (Fig. 8A–C). The probability of obtaining at least 890, 39, and 47 genes by chance (at the 0.005 level) if there are no real differences between the classes was 0.0625, 0.25, and 0.5625, respectively. Principal component analysis can be found in Fig. S8.

Discussion

Complications stemming directly from intestine/bladder incompatibilities have provided the impetus to engineer clinically relevant bladder tissue. Unfortunately, multiple studies, including two clinical trials, have failed to alleviate the significant deficit of feasible bench-to-bedside engineering approaches for bladder tissue replacement (9, 13, 14, 16, 36, 37). The premise of these clinical trials was based on the use of animal models that were anatomically and physiologically disparate from humans and utilized inflexible scaffolds (38). Clinical trial data demonstrated: an absence of statistically significant improvement in several bladder physiological measures with only a modest increase in bladder capacity; serious adverse events (bowel obstruction/bladder perforation) that led to significant morbidity requiring secondary surgeries; and bladder constructs that remained non-contractile with no evidence of functional innervation (13, 14). Thus, there still remains a great unmet clinical need to further elucidate strategies for bladder tissue regeneration.

Scaffold/bladder incompatibility has been a major obstacle in previous studies that used inelastic polymeric scaffolds [PLGA {poly(lactic-co-glycolic acid)}, PGA {poly(glycolic acid)}] (13, 14) or biological/decellularized scaffolds (39–41) that possess batch-to-batch variability with limited scalability and tunability of mechanical properties. Furthermore, SIS, for example, is a porcine-derived product that is not readily acceptable to all patient groups based on personal ideologies. CS-PRS provides several advantages over E and CS-SIS scaffolds, including bladder-like elastic mechanical properties, bio-degradability attributes, and cell-material interactions that are compatible with baboon bladder tissue regeneration and function (Fig. S9). Bladder discordant mechanical properties for the E and CS-SIS groups, coupled with DO, HN, and severe mucus accumulation in E animals, contributed to poor physiological outcomes, likely due to the inability of the graft to undergo proper bladder cycling. Early bladder cycling following augmentation has been shown to expedite tissue regeneration due to multiplanar forces encountered by the bladder that also affect cell growth and bladder shape (42–45). Fluoroscopy imaging and contour measurements (Figs. 1B and S1) demonstrated preservation of bladder shape in the CS-PRS group. In contrast, the E and CS-SIS groups all experienced a decrease in boundary regularity indicative of bladder deformation. At 50% capacity, all E and CS-SIS bladders were misshapen, indicative of graft contraction at 24 months postaugmentation (Fig. S1). Bladder shape and contour irregularities can lead to bladder dysfunction, including detrusor muscle contraction (46).

Select physiological data further highlights the utility of CS-PRS scaffolds. Although bladder capacity recovery was evident in the majority of E animals, this group experienced numerous clinical complications (HN, DO, UL, MP; Table S1) throughout the study. Persistent mucus formation was especially problematic as it can serve as a nidus for stone formation and subsequent infection (47). Mucus removal requires life-long bladder irrigation via self-catheterization. Animal M50 experienced an abnormal capacity recovery (Table S1) due to mismatched mechanical properties of intestine/bladder tissues, which we believe stemmed from hyperelastic ileum. It is unknown what the long-term effect may have been on the disposition of the animal. Animal F52 experienced multiple decreases in bladder capacity recovery, with the decrease during 18–24 months resulting in the lowest 24-month recovery across groups (38.2%). Animals in the CS-SIS group (40%) also experienced 18- to 24-month decreases, along with overall lower recovery levels (Fig. 2D). In contrast, CS-PRS animals

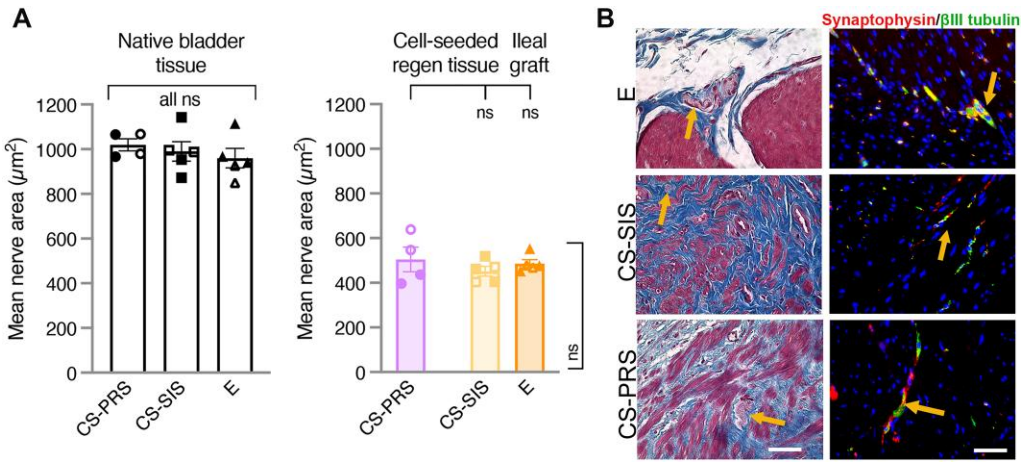

Fig. 5. Bladder tissue peripheral nerve innervation. A) Positive βIII-tubulin (neuronal element marker) staining, indicating innervation, was detected in the regenerating tissue for both CS scaffolds and in E ileal grafts, as well as in native bladder tissue. βIII-tubulin(+) nerve mean area (μm^2) was comparable in CS regenerating tissue and E ileal grafts, with all three groups showing a downshift from native bladder tissue (~0.5×) (REGEN [right graph]: CS-PRS 504.5 ± 54.8 [396.8–638.3]; CS-SIS 451.7 ± 21.8 [403.6–518.9]; E 485.9 ± 17.3 [452.5–552.6] and NATIVE [left graph]: CS-PRS 1019.6 ± 27.3 [966.1–1067.4]; CS-SIS 990.1 ± 43.8 [872.5–1142.2]; E 959.7 ± 43.4 [849.1–1114.5]). Indication of innervation in graft and regenerating tissue, along with the level of downshift from native bladder tissue, corresponds to trends in bladder strip contractile response after stimulation of nerve fibers (Fig. 7C). Data presented as mean ± SEM; $n = 4$–5 animals/group. Individual data points for each animal overlaid on corresponding bars. All ns indicate no statistically significant difference for any group comparison (CS-PRS vs. CS-SIS, CS-PRS vs. E, E vs. CS-SIS). Statistical significance (ns = not significant) determined by one-way ANOVA with Tukey–Kramer post hoc test. CS-PRS (circles) $n = 4$ animals (2M/2F); CS-SIS (squares) $n = 5$ animals (2M/3F); E (triangles) $n = 5$ animals (2M/3F). All groups, open symbols M and filled symbols F. B) The establishment of bladder peripheral nerve function is pivotal to overall bladder function. Trichrome staining demonstrated the presence of peripheral nerve bundles throughout the entirety of grafted areas of the three experimental groups depicted by orange arrows. These findings were corroborated by IF staining with synaptophysin and βIII-tubulin-specific antibodies (orange arrows). Synaptophysin and βIII-tubulin stain specifically for neural elements found in peripheral nerves. Images are representative of multiple samples/animals within a group at study termination. Blue, DAPI. Magnification is 400× (scale bar, 50 μm).

demonstrated a gradual, upward trend of bladder capacity recovery (Fig. 2C). This progressive increase in bladder capacity is important, especially in the pediatric patient population, where bladder growth should be synchronous with patient development. The clinical implications of our study are several folds and include (i) the use of nonpathological, autologous cell sources, eliminating the need for life-long immunosuppressive therapies observed in allogenic graft settings; (ii) the synthesis of a highly reproducible biosynthetic scaffold that can be produced under GMP (Good Manufacturing Practices) conditions; (iii) the direct extrapolation of the long-term baboon study to human counterparts; and (iv) the elimination of BAE procedures along with their numerous short- and long-term clinical complications.

Although the results are promising, we do acknowledge the limitations of this study. First, there is no clinically translatable animal model capable of replicating a human neurogenic bladder. While our model does not directly replicate bladder fibrosis, its current state is applicable to multiple bladder conditions that warrant BAE in order to increase capacity. These include bladder outlet obstruction, interstitial cystitis, or posterior urethral valves (36, 37, 48–50). The large deficit created by the cystectomy resembles bladder trauma experienced by wartime military personnel or those in motor vehicle accidents (51–55). Second, patients who undergo BAE typically have 24-h postsurgical care where catheters can be flushed regularly to limit mucus buildup and subsequent infection. This type of care was unavailable due to animal accessibility, although catheters were flushed several times/week until removal. Patients also provide verbal cues when in distress, which was not possible in our setting. Furthermore, all of the E animals expectedly encountered heavy MP throughout the course of the study, mimicking their human counterparts, and in some cases, this secretion contributed to infection. Animal F52 experienced a severe UTI (468 days postaugmentation), a direct consequence of the ileal graft. The length of this study was designed to simulate a phase II clinical trial in order to gather relevant long-term data. This timeframe was insufficient for peripheral nerves to reach the preaugmentation values described (Fig. 7). That said, the measured nerve function restored using CS-PRS was in line with the E group data (Fig. 7). The mean nerve area for native bladder tissue for all groups was nearly identical (~1,000 μm^2), while grafted/regenerated area values were approximately half of this value across all groups at study end (Fig. 5). In the future, this aspect of the study could be improved by providing neurotrophic factors to promote accelerated peripheral nerve regeneration and accompanying contractility. Our data demonstrate that engineered CS-PRS scaffolds promote long-term functional bladder tissue regeneration without the accompanying clinical issues observed with SIS scaffolds or BAE procedures. Finally, our previous work (21) demonstrated that human MSC/$CD34^+$ HSPC-seeded scaffold composites were superior to single-cell-seeded scaffolds with regard to bladder tissue regeneration. However, within the context of this study, it is unknown as to whether the regenerative effects are attributable to the baboon MSCs or $CD34^+$ HSPCs, or the combinatorial effects of MSC/$CD34^+$ HSPC coseeded scaffolds.

Materials and methods

PRS scaffold synthesis and characterization

The PRS scaffold, a citrate-based biomaterial, was synthesized to mimic the mechanical properties of the native baboon urinary bladder. The PRS prepolymer was synthesized by the reactions of 1,8-octanediol, citric acid, and 1-octanol at a 0.9:1.0:0.2 molar ratio. The mixture was then melted at 160 °C and reacted at 140 °C for 3 h. Purification was performed in a 20% ethanol

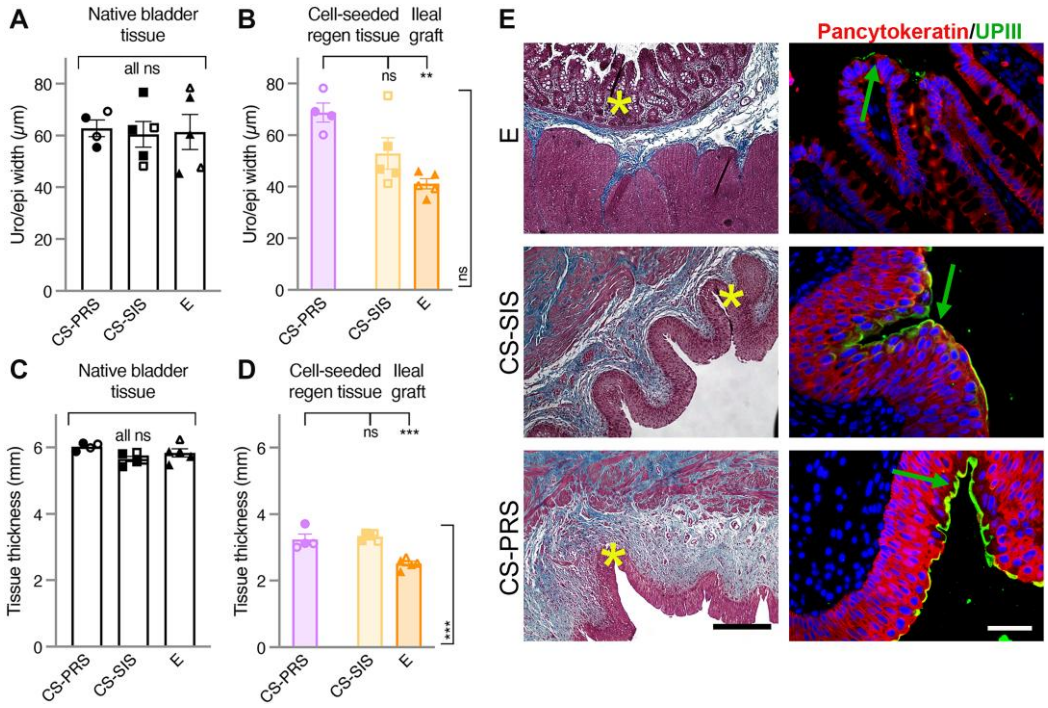

Fig. 6. Quantification of bladder tissue thickness and urothelium width. A) Mean urothelium width (μm) in native bladder tissue was similar across groups (CS-PRS 62.8 ± 3.2 [55.5–69.3]; CS-SIS 60.5 ± 4.9 [48.3–76.7]; E 61.4 ± 6.8 [45.5–78.5]). B) Mean urothelium width (μm) for regenerating tissue in CS scaffold animals was within or approaching the native bladder range, with reduced mean epithelium width (μm) in E ileal grafts reflecting the different tissue type (E 41.1 ± 2.0 [35.1–46.1] vs. CS-PRS 68.7 ± 3.7 [60.1–78.2] $^{**}P < 0.01$ [top bracket], E vs. CS-SIS 52.9 ± 6.1 [41.2–75.3] ns [side bracket]). C) Native bladder tissue thickness (mm) was comparable across groups (CS-PRS 6.0 ± 0.1 [5.9–6.1]; CS-SIS 5.7 ± 0.1 [5.4–5.9]; E 5.8 ± 0.1 [5.5–6.2]). D) Graft or regenerating tissue thickness (mm) was below the native bladder range for all three groups, with significantly lower values observed in E animals (E 2.5 ± 0.1 [2.3–2.7] vs. CS-PRS 3.2 ± 0.2 [3.0–3.7] and CS-SIS 3.3 ± 0.1 [3.2–3.4], both $^{***}P < 0.001$ [top and side brackets]). Data presented as mean ± SEM; $n = 4$–5 animals/group. Individual data points for each animal are overlaid on corresponding bars. All ns (A and C) indicate no statistically significant difference for any group comparison (CS-PRS vs. CS-SIS, CS-PRS vs. E, E vs. CS-SIS). Statistical significance ($^{**}P < 0.01$, $^{***}P < 0.001$, ns = not significant) determined by one-way ANOVA with Tukey–Kramer post hoc test. CS-PRS (circles) $n = 4$ animals (2M/2F); CS-SIS (squares) $n = 5$ animals (2M/3F); E (triangles) $n = 5$ animals (2M/3F). All groups, open symbols M and filled symbols F. E) The function of the urothelium is to provide an effective protective barrier against invading pathogens and provide an impermeable barrier against UL. This is accomplished in part by the expression and regulation of key urothelial cell proteins accompanied by proper orientation dictated by cell polarity. The failure to establish these foundational parameters can lead to abdominal and pelvic UL resulting in infection and tissue inflammation. Column I demonstrate the trichrome staining of the three experimental groups. E group animals demonstrated the presence of ileum-derived, simple columnar epithelium that was met at the interface of native bladder tissue interspersed with collagen tissue (blue). Cell-seeded grafts demonstrated robust urothelial growth as an extension from native urothelium where the urothelium width was either approaching (CS-SIS) or in the upper range of (CS-PRS) native baboon bladder tissue. This is suggestive of the combinatorial or synergistic effects of MSC/CD34$^+$ HSPCs in combination with PRS. Through surface erosion, we speculate the citric acid-related byproducts of the PRS scaffold may have rapid inductive effects on stem/progenitor urothelial cells toward self-renewal and subsequent terminal differentiation of normally quiescent urothelial stem/progenitor cells. Pancytokeratin (red)/uroplakin III (UPIII; green demarcated with green arrows) expression through IF staining (column II) was prominent in cell-seeded grafts where UPIII was absent in the epithelial layer of the ileal graft. Pancytokeratin and UPIII are proteins involved in bladder epithelial cell physiology including the regulation of membrane permeability. Images are representative of multiple samples/animals within a group at study termination. Yellow asterisks represent the area in which the IF images were taken. Blue, DAPI. Magnification-trichrome 100× and IF 400× (scale bar, trichrome 250 μm and IF 50 μm).

solution. The precipitation of the PRS prepolymer was then freeze-dried followed by dissolving in ethanol to prepare a 40% PRS prepolymer solution. The prepolymer was characterized by proton nuclear magnetic resonance (^{1}H-NMR, X500, Bruker; Fig. S10) and mass spectroscopy (AmaZon-SL, Bruker; Fig. S11) under the manufacturer's instructions.

The ^{1}H-NMR spectra were employed to study the structure of the PRS prepolymer. The peaks at 0.86 ppm were assigned to the protons in $–CH_3$ from octanol, and the multiple peaks around 2.77 ppm were assigned to the protons in $–CH_2–$ from citric acid. The composition of the prepolymer was determined by calculating the relative signal intensities of citric acid to octanol. The integral of the citric acid peak (d) was normalized to 4.00, and the integral of the octanol peak (a) was 0.56. The resulting octanol content is 18.7% close to the initial reaction feed monomer ratio (20%).

The mass distribution of PRS prepolymer resembles a bell curve with the most oligomers at 908 *m/z*, representing an oligomer with three repeat units (ru) (Fig. S11). Each ru consists of a citric acid and octanediol. There are two sets of oligomers present: one with an octanol cap and one without. The oligomers without an octanol cap represent peaks of 327 *m/z* (1 ru), 629 *m/z* (2 ru), 931 *m/z* (3 ru), 1,233 *m/z* (4 ru), and 1,535 *m/z* (5 ru). The oligomers with an octanol cap represent peaks of 741 *m/z* (2 ru), 1,043 *m/z* (3 ru), and 1,345 *m/z* (4 ru). Within each set, the separation between the peaks is 302 *m/z*, the mass of one ru, and the difference between the corresponding peaks of the sets is 112 *m/z*, the mass of octanol. The addition of each repeat unit and an octanol cap results in a condensation reaction, which is accounted for in the mass analysis. Each oligomer peak is offset by the mass of a sodium ion. One hundred milliliters of a 40% PRS solution were centrifuged to remove undissolved particles and transferred into a

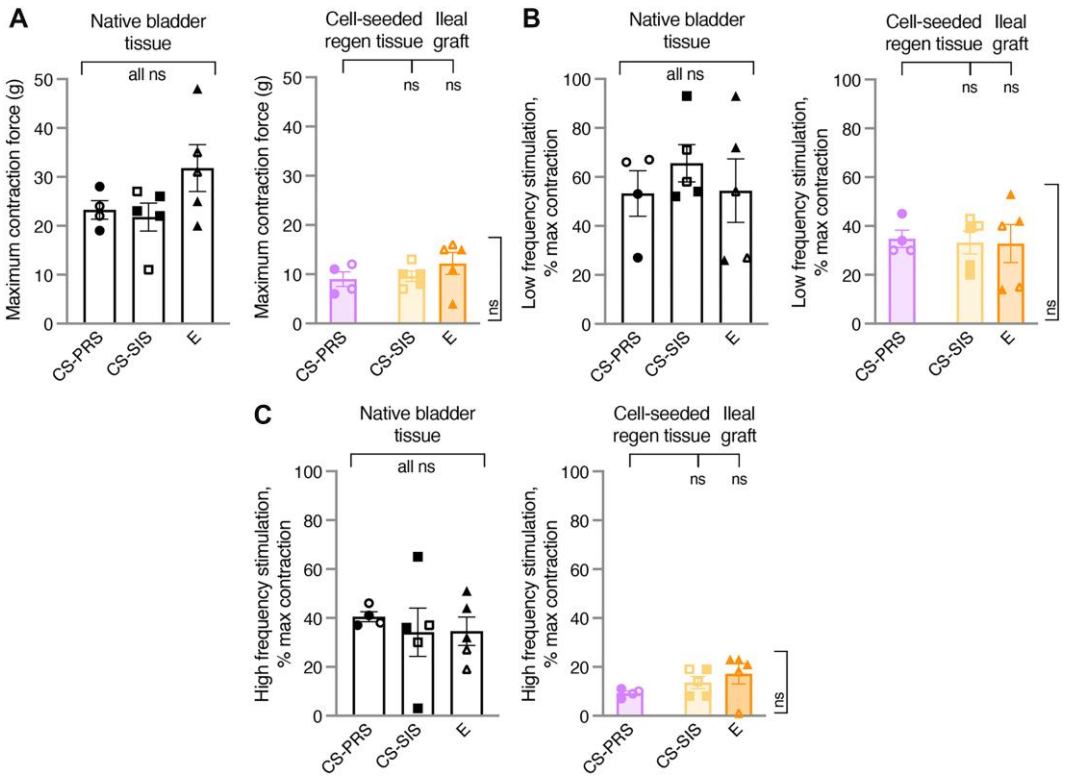

Fig. 7. Electrophysiological assessment of bladder tissue. A) For electrophysiological studies of bladder strips, smooth muscle maximum contractile force (g; MC) values were determined through stimulation with high concentration potassium chloride (KCl; depolarizes all smooth muscle cells to generate a response outside normal physiological conditions). B and C) As MC represents contractile capability beyond what can be evoked by electrical stimulation, contractions at low and high-frequency electrical stimulation are expressed as percentage of the MC elicited by high KCl stimulation (% max). Low-frequency stimulation ([LFS], [B]) preferentially activates smooth muscle, and high-frequency stimulation ([HFS], [C]) preferentially activates nerve fibers. A–C) E ileal grafts and CS regenerating tissue demonstrated responses consistent with smooth muscle contractile function and neural innervation, with no significant differences in functional physiology detected across the groups. Group means were 0.4× ([A] MC), 0.5–0.7× ([B] LFS), and 0.2–0.5× ([C] HFS) the corresponding group means for native bladder tissue. ([A] MC, NATIVE: CS-PRS 23.3 ± 1.9 [19–28]; CS-SIS 21.8 ± 2.9 [11–27]; E 31.8 ± 4.8 [20–48] and REGEN: CS-PRS 9.0 ± 1.5 [6–12]; CS-SIS 9.6 ± 1.0 [7–13]; E 12.2 ± 2.2 [4–16] [B] LFS, NATIVE: CS-PRS 53.3 ± 9.3 [27–67]; CS-SIS 65.6 ± 7.6 [52–93]; E 54.4 ± 13.0 [26–93] and REGEN: CS-PRS 34.8 ± 3.5 [30–45]; CS-SIS 33.2 ± 4.7 [20–43]; E 32.8 ± 7.8 [14–53] [C] HFS, NATIVE: CS-PRS 40.5 ± 2.0 [37–46]; CS-SIS 34.2 ± 9.9 [3–65]; E 34.6 ± 5.8 [19–51] and REGEN: CS-PRS 9.3 ± 0.9 [7–11]; CS-SIS 13.6 ± 2.5 [8–19]; E 17.2 ± 4.2 [1–23]). Data presented as mean ± SEM; $n = 4$–5 animals/group. Individual data points for each animal are overlaid on corresponding bars. All ns indicate no statistically significant difference for any group comparison (CS-PRS vs. CS-SIS, CS-PRS vs. E, E vs. CS-SIS). Statistical significance (ns = not significant) determined by one-way ANOVA with Tukey–Kramer post hoc test. CS-PRS (circles) $n = 4$ animals (2M/2F); CS-SIS (squares) $n = 5$ animals (2M/3F); E (triangles) $n = 5$ animals (2M/3F). All groups, open symbols M and filled symbols F. All groups showed a dose-dependent response to carbachol that indicated normal function of smooth muscle. Physiological studies of contractions in bladder strips provided convincing evidence that CS-PRS, CS-SIS, and E grafts demonstrated regeneration of functional smooth muscle and neural innervation. The regenerated smooth muscle was functionally normal as indicated by its response to the muscarinic agonist, carbachol. No significant differences in smooth muscle function were seen among the three groups. Measurement of smooth muscle contraction by either LFS or high potassium concentrations indicated that smooth muscle regeneration was not at the level of native smooth muscle contractile function. This reduction in contractile function indicates that smooth muscle regeneration was incomplete. HFS resulted in tissue contractions in all three graft types demonstrating strong evidence of regeneration of parasympathetic innervation. The neural reinnervation was incomplete given that the contractions were noticeably lower than the native tissues. Although present, complete smooth muscle contractility and neural reinnervation appear to require lengthier times of regeneration that go beyond the endpoints of this study which is an expected observation.

17 cm × 17 cm glass mold. The solution was left at room temperature overnight for solvent evaporation. The prepolymer was then postpolymerized at 70 °C for 5 days. Fourier transform infrared spectroscopy (FTIR, Nicolet iS50, Thermo Scientific) was used to detect the functional groups. After acquisition, the scaffold was put into DMEM (Dulbecco's Modified Eagle's Medium) medium containing 20% ethanol to leach the unreacted monomer out. The medium was changed every 8 h for an initial 24 h. Then, the scaffold was further leached in DMEM medium for 3 days with the medium changed twice a day. Finally, the scaffold was submerged in MSC Growth Media (MSCGM; Lonza Inc.) for 7 days until cell seeding. The tensile stress–strain curve of the wet scaffold was tested using an Instron universal testing machine (5,944). Briefly, the PRS scaffolds were cut into rectangular strips with a dimension of 5 cm × 1 cm and stretched at a constant velocity of 15 mm/min. To test suturability, the scaffolds were sutured onto the abdominal wall of mice followed by the removal of sutures to check if any damage occurred to the scaffold during the surgery.

The FTIR spectra of PRS scaffold confirmed the structure of the polymer (Fig. S12). The peaks at 723 and 2,929 cm^{-1} represent the bending and stretching vibrations of C–H, and the peaks at 1,178, 1,728, and 3,446 cm^{-1} represent the stretching vibrations of C–O, C=O, and O–H, respectively.

The hydrated PRS scaffold demonstrated deformability (Fig. S9A) and was more elastic than the hydrated POC [poly(1,8-octanediol-co-citrate)] scaffold based on tensile stress/strain testing (Fig. S9B). Following the suturing onto the abdominal wall of deceased mice, small cracks can be observed in the POC scaffold, but none in the PRS scaffold indicating enhanced suturability of the PRS scaffold (Fig. S9C). To test

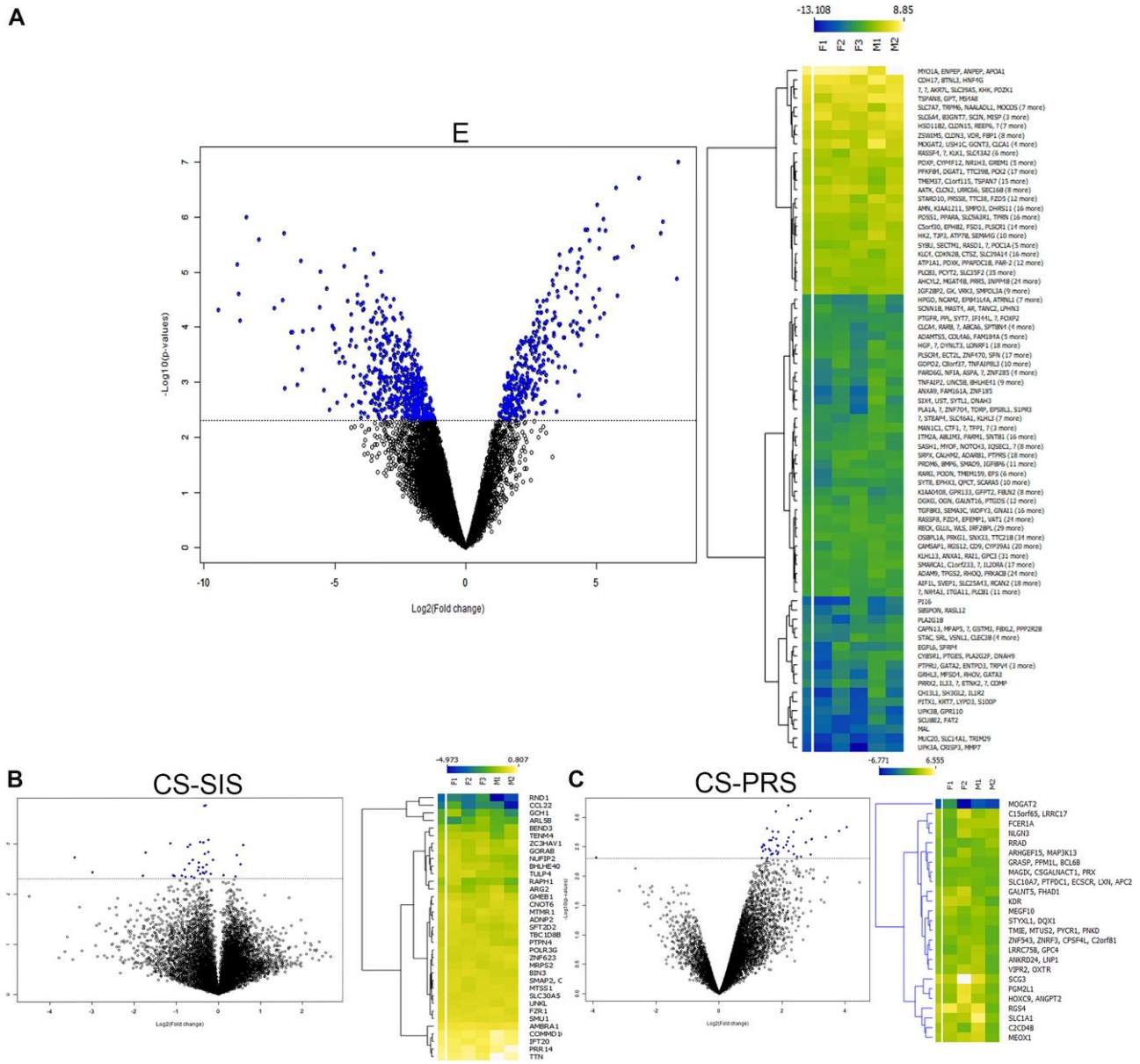

Fig. 8. Tissue transcriptome analysis. In order to demonstrate differential gene expression, volcano plots, and heat maps were generated from full-thickness tissue specimens of the three experimental groups. A–C) Volcano plot data demonstrate differentially expressed (DE) genes based on univariate paired t test between (A) native and ileal grafted tissue (E, $n = 5$ animals [F1 = animal F52, F2 = animal F54, F3 = animal F56, M1 = animal M50, M2 = animal M57]); (B) native and regenerated tissue (CS-SIS, $n = 5$ animals [F1 = animal F16, F2 = animal F17, F3 = animal F19, M1 = animal M24, M2 = animal M25]); and (C) native and regenerated tissue (CS-PRS, $n = 4$ animals [F1 = animal F20, F2 = animal F21, M1 = animal M26, M2 = animal M27]). The horizontal dotted line in each volcano plot denotes the *P*-value cutoff ($P < 0.005$ and fold-change >2.00) converted to $-\log_{10}$. Significant DE genes are denoted in blue color. The expression of specific DE genes is presented as a heat map adjacent to each respective volcano plot. DE genes with similar ratios were clustered using K means while generating the heat map. Data is presented as a $\log_2$-fold-change with genes that are downregulated depicted in blue while those that are upregulated are depicted in yellow with a transition gradient in between. Data demonstrate a statistically significant degree of gene expression similarity between native and regenerated bladder tissue in the CS-SIS and CS-PRS groups indicating that native and regenerated tissues are virtually indistinguishable at study termination. DE genes displayed in respective heat maps are of human origin upon the cluster analysis. Interestingly, several genes were found to be upregulated in these two groups including development-related genes (*MTSS1* in the CS-SIS group and *MEOX1* in the CS-PRS group) that may continue to play a downstream role in tissue regeneration/remodeling postaugmentation. Within this study, there were no consistent trends across tissue measures with regard to biological sex evident at this group size.

biocompatibility of the PRS scaffold, bone marrow-derived MSCs and $CD34^+$ HSPCs collected from baboons were seeded onto the scaffold. NucBlue Live staining demonstrated the presence of live cells via nuclei staining before respective augmentation procedures. Images are representative of multiple animals (Fig. S13).

Acknowledgments

Cell sorting was performed at the Flow Cytometry Core (FCC) Research Resources Center at the University of Illinois at Chicago. The authors acknowledge the husbandry and veterinary staff at the University of Illinois at Chicago Biologic Resources Laboratory for their expertise and dedication to this project.

Supplementary Material

Supplementary material is available at *PNAS Nexus* online.

Funding

A.K.S. discloses support for the research on this work from the National Institutes of Health (NIH) (National Institute of Diabetes and Digestive and Kidney Diseases [NIDDK], R01DK109539; National Institute of Biomedical Imaging and Bioengineering [NIBIB], R01EB026572). G.A.A. discloses support for the research of this work from the NIH (NIBIB Regenerative Engineering Training Program [RE-Training], T32-EB031527; NIBIB, R01EB026572). The content is solely the responsibility of the authors and does not necessarily represent the official views of the NIH. The authors acknowledge The Center for Advanced Regenerative Engineering (CARE) at Northwestern University and the Michelon Family and Legacy Healthcare (A.K.S.). Cell processing was performed in the Analytical BioNanoTechnology Core (ANTEC) Facility of the Simpson Querrey Institute for BioNanotechnology at Northwestern University. ANTEC is currently supported by the Soft and Hybrid Nanotechnology Experimental (SHyNE) Resource (NSF ECCS-2025633).

Author Contributions

A.K.S. conceptualized and designed the study. A.K.S., M.I.B., Y.Y.C, R.M.S., S.S.O., L.A.S., H.C.A., L.C.H., and E.Y.C. performed the baboon-related procedures. X.W., M.G.G., and G.A.A. provided oversight, prepared, and characterized PRS scaffolds. W.F. and B.G. performed FACS and analysis. K.E.M. performed bladder electrophysiological testing. N.M. and M.D.H. provided expertise and clinical oversight with regard to stem cell isolations, UDS, and interpretation, respectively. M.I.B., T.T.S., B.G.N., R.R.R., M.B., S.S.E., M.M.G., and L.W.W. conducted histological and IF tissue staining accompanied by quantitative morphometrics. M.E.S. created graphics, the surgical video, and substantial video editing. N.J.F. and M.G.G. conducted data and corresponding statistical analyses. S.L.E. performed mRNA sequencing study and computational analyses. M.I.B., N.J.F., X.W., Y.Y.C., R.M.S., T.T.S., M.M.G., L.C.H., S.L.E., M.D.H., K.E.M., G.A.A., E.Y.C., and A.K.S. wrote the manuscript.

Data Availability

The main data supporting the results in this study are available within the manuscript and its supplementary material. Sequencing datasets availability (2024 January 29) where the Metadata profile name is Bury_etal_seqDataPNAS.xlsx at the US National Center for Biotechnology Information Gene Expression Omnibus (GEO).

References

1 Rutkowski M. 1899. Zur methode der harnblasenplastik. *Zentralbl Chir*. 16:473–478.
2 Yeates WK. 1956. A technique of ileocystoplasty. *Br J Urol*. 28:410.
3 McDougal WS. 1992. Metabolic complications of urinary intestinal diversion. *J Urol*. 147:1199–1208.
4 Nurse DE, Mundy AR. 1989. Metabolic complications of cystoplasty. *Br J Urol*. 63:165–170.
5 Roth JD, Cain MP. 2018. Neuropathic bladder and augmentation cystoplasty. *Urol Clin North Am*. 45:571–585.
6 Castellan M, Gosalbez R, Bar-Yosef Y, Labbie A. 2012. Complications after use of gastric segments for lower urinary tract reconstruction. *J Urol*. 187:1823–1827.
7 Sinaiko E. 1956. Artificial bladder from segment of stomach and study of effect of urine on gastric secretion. *Surg Gynecol Obstet*. 102:433–438.
8 Roth JD, Koch MO. 2018. Metabolic and nutritional consequences of urinary diversion using intestinal segments to reconstruct the urinary tract. *Urol Clin North Am*. 45:19–24.
9 Martini A, Villari D, Nicita G. 2017. Long-term complications arising from bowel interposition in the urinary tract. *Int J Surg*. 44: 278–280.
10 Martínez-Gómez C, Angeles MA, Martinez A, Malavaud B, Ferron G. 2021. Urinary diversion after pelvic exenteration for gynecologic malignancies. *Int J Gynecol Cancer*. 31:1–10.
11 Shen JK, Chan KG, Warner JN. 2020. Continent cutaneous ileocecal cystoplasty in the treatment of refractory bladder neck contracture and urinary incontinence after prostate cancer treatment. *Can J Urol*. 27:10093–10098.
12 Jayo MJ, Jain D, Wagner BJ, Bertram TA. 2008. Early cellular and stromal responses in regeneration versus repair of a mammalian bladder using autologous cell and biodegradable scaffold technologies. *J Urol*. 180:392–397.
13 Atala A, Bauer SB, Soker S, Yoo JJ, Retik AB. 2006. Tissue-engineered autologous bladders for patients needing cystoplasty. *Lancet*. 367: 1241–1246.
14 Joseph DB, Borer JG, De Filippo RE, Hodges SJ, McLorie GA. 2014. Autologous cell seeded biodegradable scaffold for augmentation cystoplasty: phase II study in children and adolescents with spina bifida. *J Urol*. 191:1389–1395.
15 Zhang F, Liao L. 2020. Long-term follow-up of neurogenic bladder patients after bladder augmentation with small intestinal submucosa. *World J Urol*. 38:2279–2288.
16 Schaefer M, Kaiser A, Stehr M, Beyer HJ. 2013. Bladder augmentation with small intestinal submucosa leads to unsatisfactory long-term results. *J Pediatr Urol*. 9:878–883.
17 Lee J, *et al.* 2021. Mechanobiological conditioning of mesenchymal stem cells for enhanced vascular regeneration. *Nat Biomed Eng*. 5:89–102.
18 Lin H, Sohn J, Shen H, Langhans MT, Tuan RS. 2019. Bone marrow mesenchymal stem cells: aging and tissue engineering applications to enhance bone healing. *Biomaterials*. 203:96–110.
19 Kuroda R, *et al.* 2014. Clinical impact of circulating CD34-positive cells on bone regeneration and healing. *Tissue Eng Part B Rev*. 20: 190–199.
20 Malecki M, *et al.* 2013. Recruitment and retention of human autologous CD34+ CD117+ CD133+ bone marrow stem cells to infarcted myocardium followed by directed vasculogenesis: novel strategy for cardiac regeneration. *Mol Cell Ther*. 13:1–4.
21 Sharma AK, *et al.* 2013. Cotransplantation with specific populations of spina bifida bone marrow stem/progenitor cells enhances urinary bladder regeneration. *Proc Natl Acad Sci U S A*. 110: 4003–4008.
22 Bury MI, *et al.* 2021. The effects of bone marrow stem and progenitor cell seeding on urinary bladder tissue regeneration. *Sci Rep*. 11:2322–2344.
23 Bunpetch V, *et al.* 2019. Strategies for MSC expansion and MSC-based microtissue for bone regeneration. *Biomaterials*. 196: 67–79.
24 Archacka K, *et al.* 2021. Hypoxia preconditioned bone marrow-derived mesenchymal stromal/stem cells enhance myoblast fusion and skeletal muscle regeneration. *Stem Cell Res Ther*. 12:448.

25 Wang Y, *et al.* 2022. The role of gap junctions in the generation of smooth muscle cells from bone marrow mesenchymal stem cells. *Dis Markers*. 12:1491327.

26 Baberg F, *et al.* 2019. Secretome analysis of human bone marrow derived mesenchymal stromal cells. *Biochim Biophys Acta Proteins Proteom*. 1867:434–441.

27 Shin S, *et al.* 2021. Comparative proteomic analysis of the mesenchymal stem cells secretome from adipose, bone marrow, placenta and Wharton's jelly. *Int J Mol Sci*. 22:845.

28 Fierabracci A, Del Fattore A, Muraca M. 2016. The immunoregulatory activity of mesenchymal stem cells: 'state of art' and 'future avenues'. *Curr Med Chem*. 23:3014–3024.

29 Eleuteri S, Fierabracci A. 2019. Insights into the secretome of mesenchymal stem cells and its potential applications. *Int J Mol Sci*. 20:4597.

30 Yuan X, *et al.* 2022. Brain-derived neurotrophic factor is an important therapeutic factor in mesenchymal stem cell secretions for treatment of traumatic peripheral pelvic injuries. *Front Cell Neurosci*. 16:866094.

31 Matta A, Nader V, Galinier M, Roncalli J. 2021. Transplantation of CD34+ cells for myocardial ischemia. *World J Transplant*. 11: 138–146.

32 Guo X, *et al.* 2009. Correlation of CD34+ cells with tissue angiogenesis after traumatic brain injury in a rat model. *J Neurotrauma*. 26:1337–1344.

33 Zuo R, *et al.* 2019. Exosomes derived from human $CD34^+$ stem cells transfected with miR-26a prevent glucocorticoid-induced osteonecrosis of the femoral head by promoting angiogenesis and osteogenesis. *Stem Cell Res Ther*. 10:321.

34 Sharma AK, *et al.* 2011. A nonhuman primate model for urinary bladder regeneration using autologous sources of bone marrow-derived mesenchymal stem cells. *Stem Cells*. 29:241–250.

35 Caione P, Capozza N, Zavaglia D, Palombaro G, Boldrini R. 2006. In vivo bladder regeneration using small intestinal submucosa: experimental study. *Pediatr Surg Int*. 22:593–599.

36 Husmann DA. 2016. Long-term complications following bladder augmentations in patients with spina bifida: bladder calculi, perforation of the augmented bladder and upper tract deterioration. *Transl Androl Urol*. 5:3–11.

37 Hoen L, *et al.* 2017. Long-term effectiveness and complication rates of bladder augmentation in patients with neurogenic bladder dysfunction: a systematic review. *Neurourol Urodyn*. 36: 1685–1702.

38 Oberpenning F, Meng J, Yoo JJ, Atala A. 1999. De novo reconstitution of a functional mammalian urinary bladder by tissue engineering. *Nat Biotechnol*. 17:149–155.

39 Brown AL, *et al.* 2002. 22 Week assessment of bladder acellular matrix as a bladder augmentation material in a porcine model. *Biomaterials*. 23:2179–2190.

40 Lin HK, *et al.* 2014. Understanding roles of porcine small intestinal submucosa in urinary bladder regeneration: identification of variable regenerative characteristics of small intestinal submucosa. *Tissue Eng Part B Rev*. 20:73–83.

41 Ashley RA, *et al.* 2010. Regional variations in small intestinal submucosa evoke differences in inflammation with subsequent impact on tissue regeneration in the rat bladder augmentation model. *BJU Int*. 105:1462–1468.

42 Parekh A, Long RA, Iannone EC, Chancellor MB, Sacks MS. 2009. Assessing the effects of transforming growth factor-beta1 on bladder smooth muscle cell phenotype. I. Modulation of in vitro contractility. *J Urol*. 182:1210–1215.

43 Gloeckner DC, *et al.* 2002. Passive biaxial mechanical properties of the rat bladder wall after spinal cord injury. *J Urol*. 167: 2247–2252.

44 Heise RL, Parekh A, Joyce EM, Chancellor MB, Sacks MS. 2012. Strain history and TGF-β1 induce urinary bladder wall smooth muscle remodeling and elastogenesis. *Biomech Model Mechanobiol*. 11:131–145.

45 Hanczar M, Moazen M, Day R. 2021. The significance of biomechanics and scaffold structure for bladder tissue engineering. *Int J Mol Sci*. 22:12657–12690.

46 Bachelard M, Verkauskas G, Bertilsson M, Sillén UJ, Jacobsson B. 2001. Recognition of bladder instability on voiding cystourethrography in infants with urinary tract infection. *J Urol*. 166: 1899–1903.

47 Khoury AE, *et al.* 1997. Stone formation after augmentation cystoplasty: the role of intestinal mucus. *J Urol*. 158:1133–1137.

48 Baka-Ostrowska M. 2011. Bladder augmentation and continent urinary diversion in boys with posterior urethral valves. *Cent European J Urol*. 64:237–239.

49 Kim HJ, *et al.* 2014. Efficacy and safety of augmentation ileocystoplasty combined with supratrigonal cystectomy for the treatment of refractory bladder pain syndrome/interstitial cystitis with Hunner's lesion. *Int J Urol*. 21:69–73.

50 Sinha S, Shah M. 2022. Augmentation cystoplasty in children with stages III and IV chronic kidney disease secondary to neurogenic bladder. *Asian J Urol*. 9:313–317.

51 Serkin FB, *et al.* 2010. Combat urologic trauma in US military overseas contingency operations. *J Trauma*. 69:S175–S178.

52 Durrant JJ, Ramasamy A, Salmon MS, Watkin N, Sargeant I. 2013. Pelvic fracture-related urethral and bladder injury. *J R Army Med Corps*. 159:i32–i39.

53 Mahat Y, Leong JY, Chung PH. 2019. A contemporary review of adult bladder trauma. *J Inj Violence Res*. 11:101–106.

54 Singer G, Arneitz C, Tschauner S, Castellani C, Till H. 2021. Trauma in pediatric urology. *Semin Pediatr Surg*. 30:151085–151092.

55 Coccolini F, *et al.* 2019. WSES-AAST expert panel. Kidney and urotrauma: WSES-AAST guidelines. *World J Emerg Surg*. 14:54–107.